J Mater Sci (2008) 43:1669–1676
DOI 10.1007/s10853-007-2387-y

Photochemical synthesis and characterization of Ag/TiO_2 nanotube composites

Haibin Li · Xuechen Duan · Guocong Liu · Xiaoqi Liu

Received: 29 June 2007 / Accepted: 5 December 2007 / Published online: 11 January 2008

Abstract TiO_2 nanotubes were fabricated by a hydrothermal method. Silver nanoparticles with diameters around 3–5 nm were loaded onto the surface of TiO_2 nanotubes via a deposition approach followed by a photochemical reduction process under ultraviolet irradiation. Transmission electron microscopy (TEM), N_2 adsorption measurements, X-ray diffraction (XRD), X-ray photoelectron spectroscopy (XPS), Raman spectroscopy, UV-vis diffuse reflectance spectroscopy (UV-vis), and fluorescence spectroscopy (FL) were applied to characterize the as-prepared Ag/TiO_2 nanotube composites. The photocatalytic activity of the as-prepared materials was investigated by photodegrading of methyl orange. The results showed that silver particles were in zero oxidation state and highly dispersed on the surface of TiO_2 nanotubes when the concentration of Ag^+ was low. The presence of metallic silver can help the electron-hole separation by attracting photoelectrons. The Ag/TiO_2 nanotube composites with a suitable amount of silver showed a further improvement on the photocatalytic activity for degradation of methyl orange in water.

Introduction

Titanium dioxide is a wide-bandgap semiconductor. Application of heterogenous photocatalysis with nanostructure TiO_2 to waste water treatment has been profoundly studied over the past several decades. It has attracted much interest due to its nontoxicity, low cost, friendly operation conditions, and significantly low energy consumption. However, the high recombination rate of photogenerated electron/hole pairs of TiO_2 and wide bandgap results in the low photocatalytic efficiency.

In resent decades, great efforts have been made on the fabrication and application of nanocrystals due to their different chemical and physical properties from those of bulk materials. The properties of nanomaterials are greatly affected by their size and morphology. One-dimensional (1D) nanostructured materials have become one of the hottest research fields, as the anisotropic morphology of one-dimensional (1D) nanostructure makes it exhibit superior optical, magnetic, electrical, and mechanical properties [1]. One-dimensional (1D) TiO_2 nanostructures, such as nanorods [2, 3], nanofibers [4], and nanotubes [5] are promising photocatalysts with higher activities than those of nanoparticles. TiO_2 Nanotubes are particularly interesting because of their larger surface area and pore volume. Various methods, including anodic oxidation, template technique [6], and hydrothermal synthesis [7], have been applied to prepare titanium dioxide nanotubes. Hydrothermal process is especially attractive due to its facility to fabricate uniform TiO_2–NTs (nanotubes) with an external diameter around 10 nm [8].

Although TiO_2 nanotubes are much more active than TiO_2 nanoparticles in photocatalysis, the drawbacks mentioned above still exist. The previous works [9–15] have proven that many attempts, including combination of TiO_2 with other semiconductors, doping with impurities, and partially coating with noble metals, could effectively enhance the photocatalytic activity of TiO_2. TiO_2–NTs-supported gold [16, 17], copper [17], Pt [18, 19], Pd [20],

H. Li (✉) · X. Duan · G. Liu · X. Liu
School of Materials Science and Engineering, Central South University, Changsha 410083, People's Republic of China
e-mail: coastllee@hotmail.com

G. Liu
Department of Chemistry, Yulin Normal University, Yulin 537000, People's Republic of China

and Ru [18, 21] photocatalysts have been successfully synthesized. Ag/TiO_2 nanoparticle composite has been profoundly investigated over past several decades [22–27], but few works focus on the silver-modified TiO_2–NTs catalyst by now. Silver is a promising noble metal that is often applied to modify TiO_2 promoting photocatalytic effectiveness of TiO_2. Silver deposition particles can act as electron trapper to slow down the rate of electron-hole recombination, thus more holes are available for the oxidation reactions. Furthermore, the relative low cost compared to other noble metals, bactericidal property [28], and special behavior for oxygen adsorption [26] make silver a better choice for modification of TiO_2–NTs. In most previous works, silver deposits were fabricated by reduction of Ag^+ using UV irradiation [23, 26, 27, 29]. The way is facile, but it is not easy to produce uniform silver clusters that have very small diameters and strongly anchor on the surface of TiO_2.

Herein we report the synthesis of Ag/TiO_2 nanotube composites via a deposition approach followed by a photochemical reduction process under UV irradiation. Transmission electron microscopy (TEM), N_2 adsorption measurements, X-ray diffraction (XRD), X-ray photoelectron spectroscopy (XPS), Raman spectroscopy, UV-vis diffuse reflectance spectroscopy (UV-vis), and fluorescence spectroscopy (FL) were applied to characterize the products. Tests of photocatalytic activity of the samples were performed by photodegrading methyl orange in water.

Experimental

Reagents

Titanium dioxide, anatase (TiO_2), sodium hydroxide (NaOH), nitric acid (HNO_3), silver nitrate ($AgNO_3$), hydrochloric acid (HCl), and methyl orange (MO). All chemicals were of analytical grade and used without further purification.

Synthesis of TiO_2 nanotubes

The TiO_2 nanotubes were synthesized following a literature procedure [7, 8]. Briefly, one gram of titanium dioxide (TiO_2) was mixed with 40 mL 10 M sodium hydroxide (NaOH) aqueous solution. The whole mixture was stirred for 3 h before it was transferred into a 50 mL Teflon-lined stainless steel autoclave, sealed, and then heated at 408 K for 24 h. The prepared white powder was treated with 0.1 M hydrochloric acid (HCl) solution, then further washed with distilled water repeatedly, followed by vacuum-drying at 333 K for 6 h. The product was finally calcined at 673 K in air for 1 h.

Synthesis of Ag/TiO_2 nanotube composites

The fabrication of Ag/TiO_2 composites was conducted as follows. First, a given amount of silver nitrate ($AgNO_3$) was dissolved in 200 mL of distilled water. 0.80 g of TiO_2–NTs was dispersed in this solution under stirring. The pH of the suspension was adjusted to two using 1 M nitric acid (HNO_3). After ultrasonically treated for 30 min the suspension was further magnetically stirred for 24 h in the dark. Then 0.3 M sodium hydroxide (NaOH) solution was added dropwise into the suspension until the pH was 12, followed by UV illumination for 4 h under stirring. The black powder was centrifuged, rinsed with distilled water repeatedly to purify the product, and finally dried at 333 K under vacuum.

Characterization of Ag/TiO_2 nanotube composites

The morphology of the samples was investigated by transmission electron microscopy (TEM, Philips Tecnai 20 G2 S-TWIN). The Brunauer–Emmett–Teller (BET) surface area of the samples was obtained from Nitrogen adsorption isotherms (Micromeritics, ASAP-2020). The crystalline phase was identified by X-ray diffraction (XRD) using a Rigaku D/Max 2500 powder diffractometer with Cu Kα radiation ($\lambda = 1.5406$ Å). X-ray photoelectron spectroscopy (XPS) data of the samples were obtained with an ESCALab220i-XL electron spectrometer from VG Scientific using 300 W Al Kα radiation. Raman spectrum of the sample was measured with RFS100/S FT-Raman apparatus from Bruker. UV-vis diffuse reflectance spectroscopy analysis (UV-vis) was performed on a Specord 200 UV spectrophotometry. Fluorescence spectroscopy analysis (FL) of the as-prepared samples was carried out on a Hitachi F-4500 Fluorescence Spectrophotometer.

Tests of photocatalytic activity

The photocatalytic properties of Ag/TiO_2 nanotube composites were assessed by photodegradation of methyl orange aqueous solution. One hundred milliliters of 10 mg L^{-1} methyl orange aqueous solution (pH = 2) was mixed with 0.2 g photocatalyst. The mixture was magnetically stirred in dark for 30 min before commencing the photocatalytic reactions to allow the system to reach adsorption/desorption equilibrium. All photocatalytic reactions were carried out in a laboratory-constructed photoreactor under ultraviolet irradiation with a 125 W ultraviolet lamp (peak wavelength at 365 nm). The photocatalytic system was magnetically stirred simultaneously during the course of illumination. The concentrations of

methyl orange solution were evaluated by an UNICO UV-2100 spectrophotometer at 508 nm.

Results and discussion

TEM and BET analysis

The TEM images of neat TiO_2 nanotubes and Ag/TiO_2 nanotube composites after UV irradiation for 4 h are exhibited in Fig. 1. Figure 1a shows the image of neat TiO_2 nanotubes calcined at 673 K, a large number of open-ended TiO_2–NTs with uniform diameters around 10 nm and lengths about several hundreds can be clearly seen in the picture. No obvious damage is found and the materials remain in good shape. The overall view of silver-coated nanotubes with Ag/TiO_2 atomic ratios of 2.0% is presented in Fig. 1b. TiO_2 nanotubes maintain tubular structure. Silver particles with diameter less than 5 nm highly disperse on the surface of TiO_2–NTs. No "support-free" silver particles are found in the resulting silver-coated TiO_2–NTs, indicating that the silver particles are strongly anchored to the supports. During the deposition process, TiO_2–NTs act as supports to adsorb silver precursors because of their large surface area. As the silver precursors assemble onto the TiO_2–NTs, their aggregation tendency is also prevented when the density of silver is low and the silver deposition process is very slow. Then evenly dispersed silver nanoparticles can be readily obtained after the UV irradiation process. However, by increasing the concentration of Ag^+, both the density of Ag particles on the surface of TiO_2–NTs and the size of silver particles increase. In Fig. 1c, it can be observed that lots of silver particles have diameter around 10 nm, some even have diameter larger than 10 nm. Moreover, lots of particles aggregate and cover a large part of the surface of TiO_2–NTs. When the concentration of Ag^+ further increases to at.10%, some "support-free" silver particles with diameter about 40 nm appear and the major part of TiO_2–NTs are coated by silver, as illustrated in Fig. 1d. It can be concluded that both the

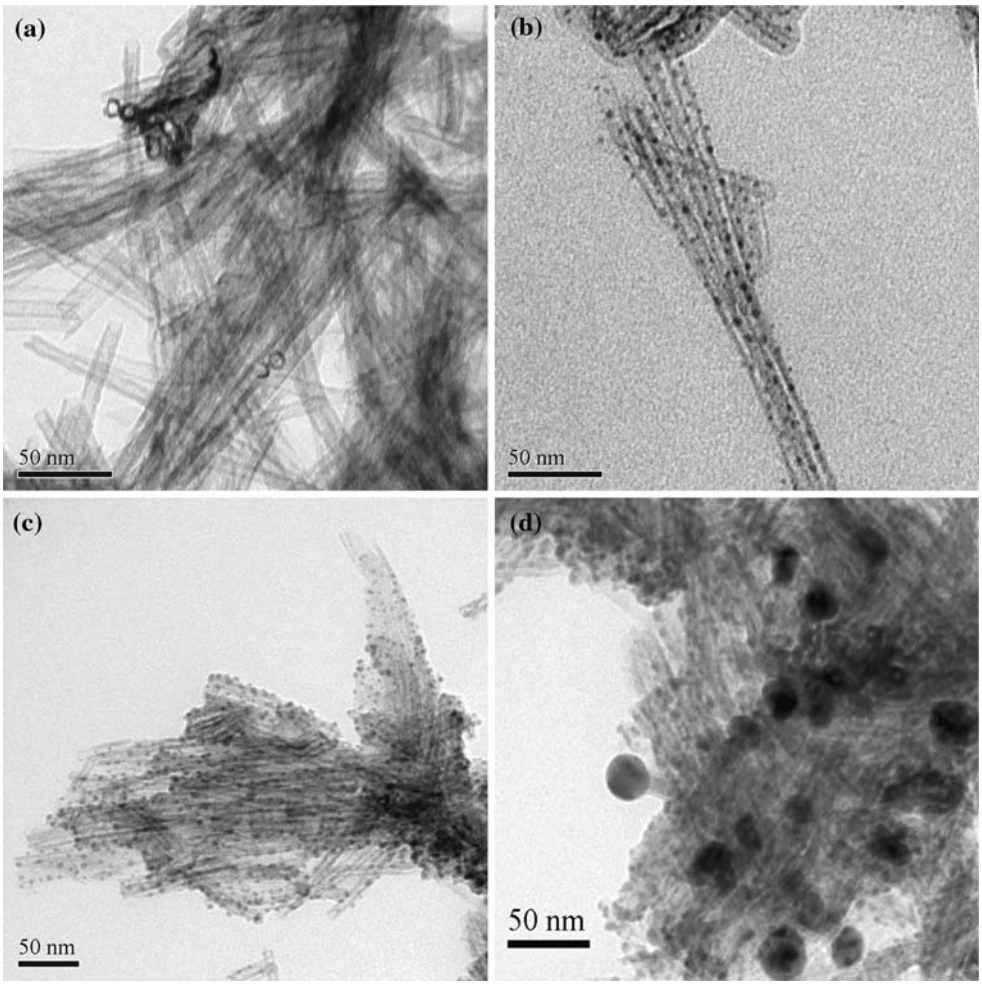

Fig. 1 TEM images of neat TiO_2 nanotubes (**a**) and Ag/TiO_2 nanotube composites with the Ag/TiO_2 atomic ratio of 2% (**b**), 5% (**c**), and 10% (**d**)

concentration of Ag^+ and the precise control of the deposition process are very important for fabrication of silver nanoparticles with diameter less than 5 nm and high dispersity on the surface of TiO_2–NTs.

It should be noted that silver ions might be adsorbed onto both outer and inner surfaces of nanotubes due to the pore structure of TiO_2–NTs. The formation of silver particles will occur on the inner wall of TiO_2–NTs, which may decrease the pore volume of TiO_2–NTs and result in the decline of surface area of nanotubes. As measured by N_2 adsorption measurements, the BET surface area of neat TiO_2–NTs is 223.7 $m^2\ g^{-1}$, while the areas of the composites with Ag/TiO_2 atomic ratios of 2.0% and 5.0% are 201.3 $m^2\ g^{-1}$, and 187.4 $m^2\ g^{-1}$, respectively. The higher the Ag is loaded, the larger the decrease in the BET surface area of the samples. It indicates that more and more silver particles are assembled onto the both surfaces of nanotubes and occupy the pore space with increasing the loading amount of Ag.

X-ray diffraction investigation

XRD results of neat TiO_2 nanotubes and Ag/TiO_2 nanotube composites with the Ag/TiO_2 atomic ratios of 5% and 10% are shown in Fig. 2. It can be seen from Fig. 2 that for all the samples, only characteristic peaks corresponding to anatase phase are found, no other crystalline species of TiO_2 was detected by XRD. In addition, any characteristic peaks resulted from silver cannot be seen in Fig. 2 although the Ag/TiO_2 atomic ratio of the heaviest silver-coated TiO_2–NTs is 10%. Since the silver particles were originated from Ag_2O which was prepared by deposition of Ag^+ from $AgNO_3$ aqueous solution, neither Ag_2O nor Ag were heat treated, it is most likely that the silver particles are amorphous. In the previous work [30, 31], it was reported that silver particles with good crystallinity could be readily obtained after calcination of Ag-coated TiO_2. However, we found that the heat treatment of Ag/TiO_2–NTs composites could result in the aggregation of silver particles, which might reduce the activity of the catalyst. So we chose the crystallized TiO_2–NTs as the support of silver particles to avoid the further thermal treatment of the products.

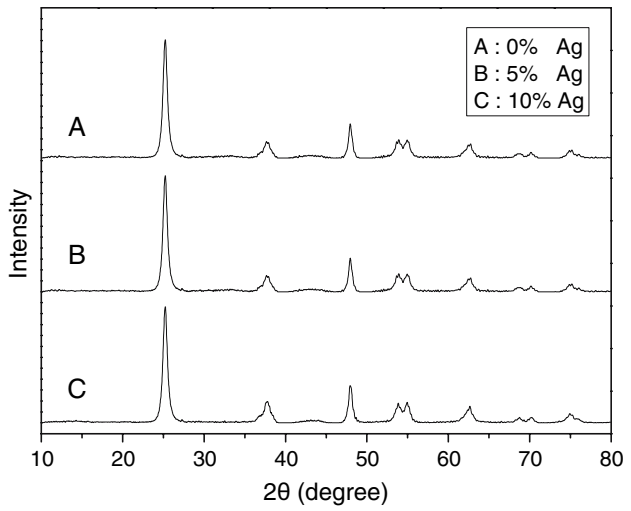

Fig. 2 XRD patterns of neat TiO_2 nanotubes and Ag/TiO_2 nanotube composites with different Ag/TiO_2 atomic ratios

XPS and Raman analysis

The TEM images show that the silver nanoparticles are strongly anchored to TiO_2–NT, but the XRD results give no information about the silver nanoparticles. To further study the state of the silver nanoparticles and make it clear whether the silver nanoparticles are in zero oxidation state or a mixture of Ag and Ag_2O, the Ag/TiO_2–NT composites sample after UV irradiation for 4 h was subjected to X-ray photoelectron spectroscopy and Raman spectroscopy analysis. Figure 3 shows the XPS spectra of Ti2p (Fig. 3a), O1s (Fig. 3b), and Ag3d (Fig. 3c). As depicted in Fig. 3a, binding energies of 458.3 ev and 463.9 ev correspond to the peaks of $Ti2p_{3/2}$ and $Ti2p_{1/2}$, respectively. They are assigned to the lattice of titanium in titanium oxide corresponding to a 2p3 binding energy of Ti(IV) ion. The O1s XPS spectrum for the Ag/TiO_2 composites shows a narrow and sharp peak structure and has a binding energy of 529.7 ev which is ascribed to the chemical bonding of O1s–Ti state, as illustrated in Fig. 3b. Kuo [32] reported that the XPS spectrum of O1s for Ag-modified TiO_2 coating showed a broad structure and a peak at 529.2 ev appeared when there was a silver species of Ag_2O. However, no peaks matching the chemical bonding of O1s–Ag have been found in Fig. 3b, illustrating the absence of any silver oxides species. Figure 3c provides further evidence of the zero oxidation state of silver particles. As presented in Fig. 3c, the XPS spectra in the Ag3d region consisted of two peaks at 368.10 ev and 374.10 ev, which correspond to $Ag3d_{5/2}$ and $Ag3d_{3/2}$, respectively. It can be inferred from Fig. 3c that the silver species on the Ag/TiO_2 composites is metallic silver in terms of the bonding energy corresponding to $Ag3d_{5/2}$ of Ag (Ag^0, 368.25 ev) and Ag_2O (Ag^+, 367.70 ev) [33]. The Ag3d XPS peaks are in good agreement with the O1s XPS result of the absence of Ag_2O particles on the Ag/TiO_2 composites.

Raman spectroscopy was also applied in order to study the structure of silver nanoparticles anchoring inside the nanotubes. Figure 4 shows the Raman spectrum of Ag/TiO_2–NT composites. The spectrum is identical to that of pure anatase TiO_2, which indicates that loading of Ag

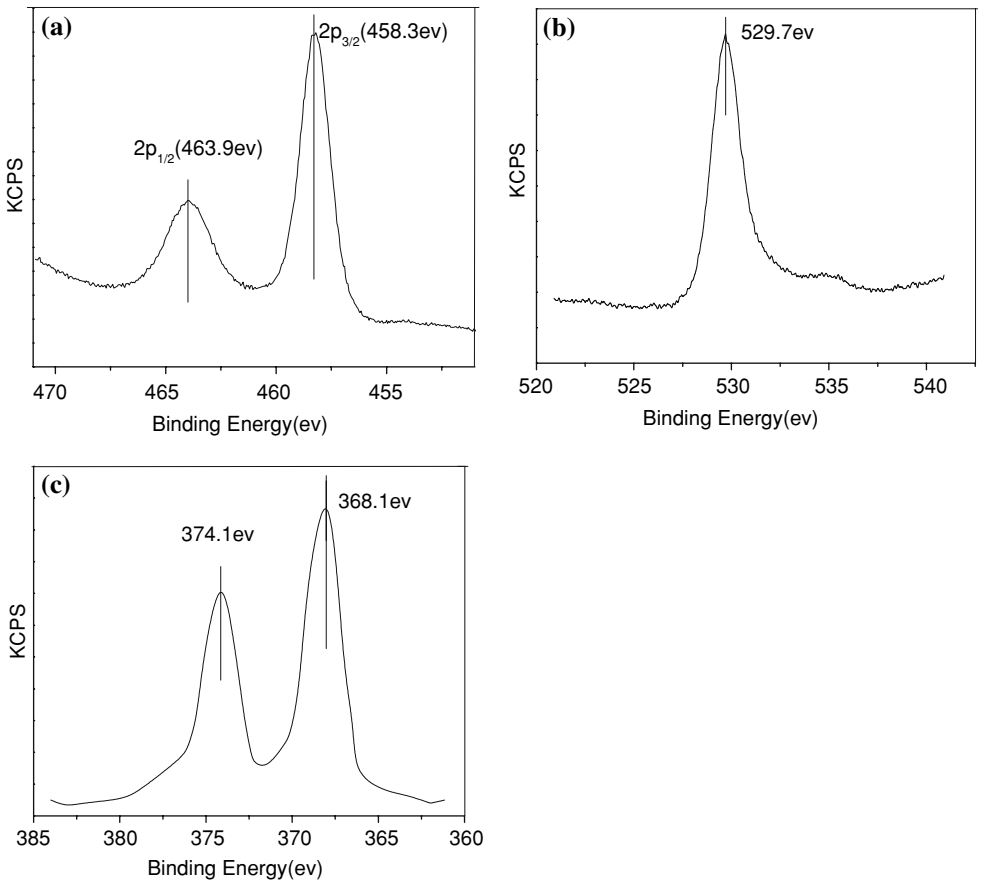

Fig. 3 XPS spectra of Ti2p (**a**), O1s (**b**), and Ag3d (**c**)

particles has no effects on the microstructure of TiO_2–NTs. We also note that any species of silver oxides are not found in the spectrum, illustrating that Ag_2O particles assembled on TiO_2–NTs surface are totally reduced after UV irradiation for 4 h.

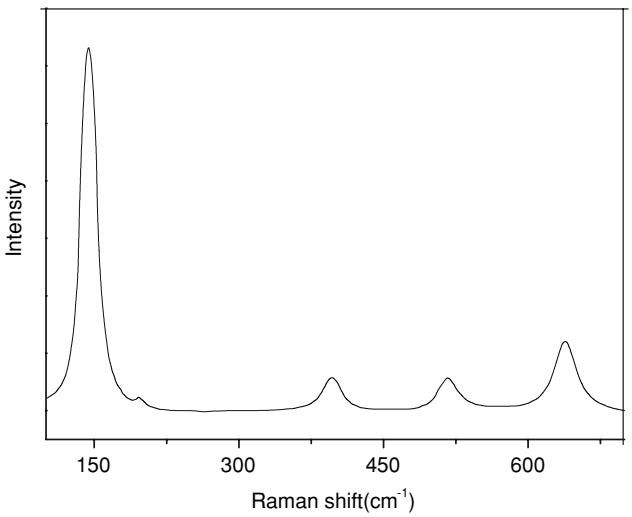

Fig. 4 Raman spectrum of Ag/TiO_2–NT composites

UV-vis diffuse reflectance spectra analysis

The room temperature UV-vis diffuse reflectance spectra of neat TiO_2–NTs and Ag/TiO_2 nanotube composites are presented in Fig. 5. As can be seen from curve A in Fig. 5, neat TiO_2 nanotubes have a broad intense absorption below ca. 400 nm. It is the characteristic absorption of TiO_2 corresponding to the charge transfer process from the valence band to conduction band in anatase TiO_2. When Ag_2O-assembled TiO_2–NTs was illuminated by UV light, the color of the product changed to black. This indicated the decomposition of Ag_2O. In the UV-vis spectra of the Ag/TiO_2 composites, it can be seen that there is a strong absorption peak around 445 nm in the visible range. This is the characteristic of surface plasmon absorption corresponding to Ag^0 particles [31, 34], illustrating the successful reduction of Ag_2O. The UV-vis spectrum of the Ag/TiO_2 composites is in good agreement with the Ag3d XPS result. As for the TiO_2 catalyst, the modification is usually performed by two ways. The one is the decrease in bandgap energy of TiO_2 to make use of solar lights; the other is the effective separation of electrons and holes. The effect of sliver on the band energy of TiO_2–NTs is inferred from its UV-vis spectra analysis result that coating of silver

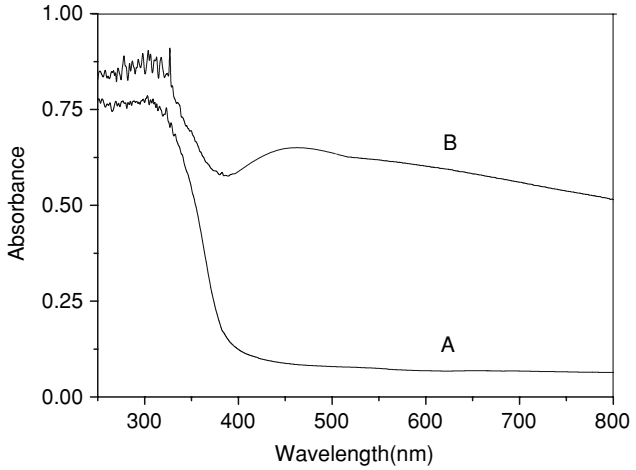

Fig. 5 UV-vis diffuse reflectance spectra of neat TiO_2–NT (**a**) and Ag/TiO_2 nanotube composites (**b**)

nanoparticles on TiO_2 nanotubes has few effects on the band energy of TiO_2.

Fluorescence spectroscopy test

In order to realize the function of silver nanoparticles on TiO_2–NTs and investigate their efficiency of electron/hole separation, the products were subjected to the fluorescence spectra analysis. In Fig. 6, it can be seen that the fluorescence intensities of silver-loaded TiO_2 nanotubes are lower than those of neat TiO_2–NTs. Moreover, on increasing the loaded amount of silver, the FL intensity of Ag/TiO_2–NTs decreases. Tseng reported the similar phenomena in copper-doped TiO_2 photocatalyst that the doped catalyst showed lower FL intensity comparing with the pure TiO_2 [35]. The previous studies suggested that the fluorescence of TiO_2 is generated by the recombination of photoexcited electrons and holes. The lower fluorescence intensity is due to the smaller number of recombination sites on the surface of TiO_2–NTs. It can be concluded that silver clusters on the surface of TiO_2–NTs behave as electrons trappers and effectively inhibit the recombination of electrons and holes, thus the decline of the FL intensity.

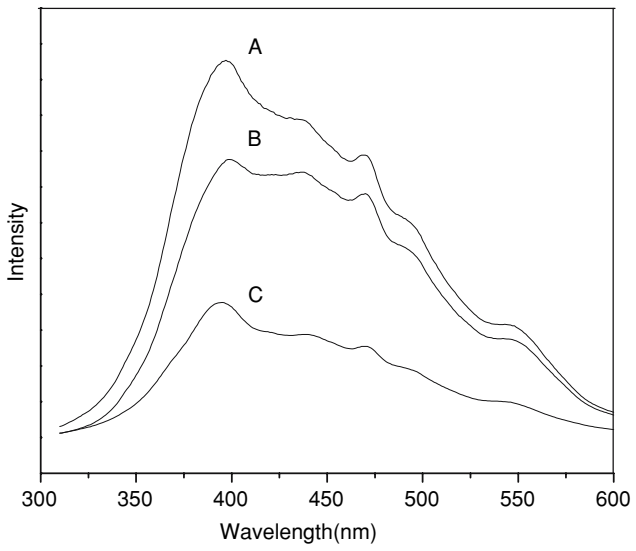

Fig. 6 The fluorescence spectra of neat TiO_2–NT (**a**) and Ag/TiO_2–NTs composites with the Ag/TiO_2 atomic ratios of: 1% (**b**), 2% (**c**), respectively

Deposition of silver nanoparticles onto the surface of TiO_2 nanotubes

The deposition process of Ag nanoparticles onto TiO_2–NTs surface is illustrated in Fig. 7. First, a given amount of TiO_2–NTs is dispersed in $AgNO_3$ acid aqueous solution of a certain concentration to obtain a suspension, followed by a strong magnetic stir for 24 h in the dark. Silver ions are then adsorbed onto both outer and inner walls of TiO_2–NTs. It has to be noted that adsorption of Ag^+ onto the inner surface of TiO_2–NTs is weaker than that onto the outer surface due to the inconvenience of silver ions to travel into nanotubes and smaller area of inner surface.

$$Ag^+ \rightarrow Ag^+_{adsorbed} \quad (1)$$

A given amount of 0.3 M NaOH aqueous solution is then added into the foregoing suspension to totally deposit the adsorbed Ag^+ onto the surface of TiO_2–NTs.

$$2Ag^+_{adsorbed} + 2OH^- \rightarrow Ag_2O \downarrow + H_2O \quad (2)$$

Subsequently, the resulted Ag_2O particles are reduced into metallic silver by an ultraviolet irradiation. As for the Ag_2O particles locating inside TiO_2–NTs, the porous channels of TiO_2–NTs which allow UV light penetration are favorable for their reduction.

$$2Ag_2O \xrightarrow{hv} 4Ag + O_2 \uparrow \quad (3)$$

It is interesting to mention that UV light induced free electrons which transfer from the valence band to the conduction band in TiO_2 catalyst are also helpful for the photochemical synthesis of Ag/TiO_2–NTs, especially for the decomposition of Ag_2O nanoparticles locating inside the nanotubes, as illustrated by the following reactions:

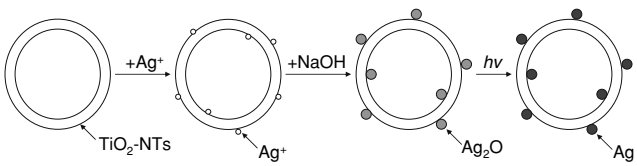

Fig. 7 A schematic diagram of the process for fabricating Ag/TiO_2–NT composites

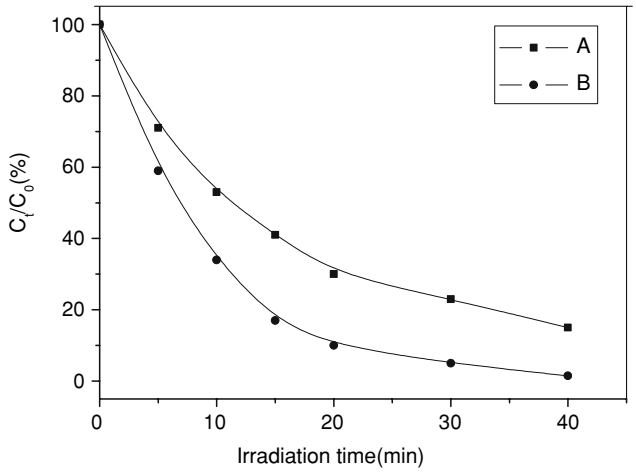

Fig. 8 Photocatalytic efficiency of silver-coated TiO_2 nanoparticles and Ag/TiO_2–NT composites with the same Ag/TiO_2 atomic ratio of 2%

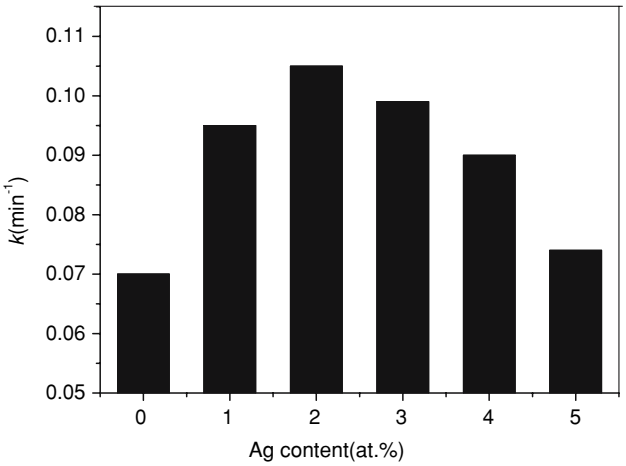

Fig. 9 The dependence of the rate of methyl orange degradation on the silver level in Ag/TiO_2–NT composites photocatalytic system

$$TiO_2 \xrightarrow{hv} h^+ + e^- \quad (4)$$

$$Ag_2O + e^- \longrightarrow Ag \quad (5)$$

Photocatalytic activity for degradation of methyl orange in water

Figure 8 displays the photocatalytic efficiency of Ag/TiO_2–NT composites catalyst. For comparison, the photocatalytic performance of silver-coated TiO_2 nanoparticles was also investigated under the same experimental conditions. The TiO_2 nanoparticles were synthesized following a literature procedure [20] with $Ti(OBu)_4$ as Ti source, while silver-coated TiO_2 nanoparticles were prepared applying the same method mentioned in 2. 3. The plot shows that silver-coated TiO_2–NTs are more active than silver-coated TiO_2 nanoparticles for photodegradation of methyl orange, which should be attributed to the larger surface area and pore volume of nanotubes.

To further understand the effect of silver content on the photocatalytic activity of Ag/TiO_2 nanotube composites, we investigated the dependence of rate of methyl orange degradation on the silver level, which is displayed in Fig. 9. The photocatalytic reaction rate constant k was calculated according to the following formula [15]: $\ln(C_0/C_t) = kt$, where C_0 and C_t are the concentrations of methyl orange in the primary stage of experiment and after t minutes UV irradiation [36]. As shown in Fig. 9, k first increases with the increasing atomic ratio of Ag/TiO_2, and then reaches to an optimum value when the atomic ratio of Ag/TiO_2 is 2.0%. Further increasing the amount of silver beyond this level shows harmful effects on the photodegradation of methyl orange.

The higher photocatalytic efficiency of Ag/TiO_2 composites may be ascribed to the fact that silver particles on the surface of TiO_2–NTs can facilitate the charge separation by attracting photoelectrons, thus more holes are available for the oxidation of organic.

$$TiO_2 \xrightarrow{hv} e^- + h^+ \quad (6)$$

$$Ag + e^- \rightarrow Ag^{\bullet -} \quad (7)$$

$$H_2O + h^+ \rightarrow H^+ + OH^{\bullet} \quad (8)$$

$$OH^{\bullet} + MO \rightarrow CO_2 + H_2O \quad (9)$$

However, the excess laded content of silver particles may cover a large part of the surface of TiO_2–NTs, as observed in Fig. 1c,d, decreasing the active sites on the TiO_2 surfaces. In addition, excess coverage of silver deposits may reduce the access of UV irradiation to the surface of TiO_2–NTs, thus there is decrease in photogenerated carriers and low photocatalytic activity. Moreover, with increasing the silver loading, more and more silver clusters load onto the surface of TiO_2–NTs and aggregate, as presented in Fig. 1, which makes the energetic properties of the loaded silver approach to that of bulk silver [22]. It is more likely for the loaded silver to play a role as electron-hole recombination center rather than an electron trapper.

$$Ag + e^- \rightarrow Ag^{\bullet -} \quad (10)$$

$$Ag^{\bullet -} + h^+ \rightarrow Ag \quad (11)$$

It can be concluded that both the content and the dispersity of silver particles are crucial factors to the photocatalytic activity of Ag/TiO_2 nanotube composites.

Conclusion

In summary, we demonstrated a simple deposition method followed by a photochemical reduction process to prepare

Ag/TiO_2 nanotube composites. It was found that silver particles with diameters of less than 5 nm were evenly loaded onto the surface of TiO_2–NTs when the concentration of Ag^+ is low. The photochemical reduction of silver particles from Ag_2O to Ag^0 was proved by XPS, Raman, and UV-vis spectra. The as-prepared composites with a suitable content of silver showed a higher photocatalytic activity than those of pure TiO_2–NTs. Silver deposits on TiO_2–NTs surface effectively act as electron trappers inhibiting the electron-hole recombination. The better separation of photogenerated electrons and holes allows more efficiency for photodegradation of methyl orange.

Acknowledgements The authors acknowledge the financial support from Science and Technology Bureau of Hunan Province (No.01JJY20575), Science and Technology Bureau of Guangdong Province (No.2006D90404033), and Science and Technology Bureau of GuangXi Province (No.0728107). We also would like to thank Waytech nanotechnology Ltd. for the assistance.

References

1. Xia Y, Yang P, Sun Y, Wu Y, Mayers B, Gates B, Yin Y, Kim F, Yan H, (2003) Adv Mater 15:353
2. Li X-L, Peng Q, Yi J-X, Wang X, Li YD (2006) Chem-Eur J 12:2383
3. Limmer SJ, Chou TP, Cao GZ (2004) J Mater Sci 39:895
4. Li D, Xia YN (2003) Nano Lett 3:555
5. Mor GK, Shankar K, Paulose M, Varghese OK, Grimes CA (2005) Nano Lett 5:191
6. Sander MS, Cote MJ, Gu W, Kile BM, Tripp CP (2004) Adv Mater 16:2052
7. Kasuga T, Hiramatsu M, Hoson A, Sekino T, Niihara K (1999) Adv Mater 11:1307
8. Yuan Z-Y, Su B-L (2004) Colloid Surf A 241:173
9. Arpac E, Sayılkan F, Asiltürk M, Tatar P, Nadir Kiraz, Sayılkan H (2007) J Hazard Mater 140:69
10. Dvoranová D, Brezová V, Mazúra M, Malati MA (2002) Appl Catal B Environ 37:91
11. Burda C, Lou YB, Chen XB, Samia ACS, Stout J, Gole JL (2003) Nano Lett 3:1049
12. Zhang DR, Kim YH, Kang YS (2006) Curr Appl Phys 6:801
13. Kim SC, Heo MC, Hahn SH, Lee CW, Joo JH, Kim JS, Yoo Ik-K, Kim EJ (2005) Mater Lett 59:2059
14. Moon Jooho, Takagi H, Fujishiro Y, Awano M (2001) J Mater Sci 36:949
15. Hou LR, Yuan CZ, Peng Y (2007) Hazard J Mater 139:310
16. Xu J-Z, Zhao W-B, Zhu J-J, Li G-X, Chen H-Y (2005) J Colloid Interf Sci 290:450
17. Zhu BL, Guo Q, Huang XL, Wang SR, Zhang SM, Wu SH, Huang WP (2006) J Mol Catal A Chem 249:211
18. Macak JM, Barczuk PJ, Tsuchiya H, Nowakowska MZ, Ghicov A, Chojak M, Bauer S, Virtanen S, Kulesza PJ, Schmuki P (2005) Electrochem Commun 7:1417
19. Nam W, Han GY (2007) J Chem Eng Jpn 40:266
20. Wang M, Guo D-j, Li H-l (2005) J Solid State Chem 178:1996
21. Bavykin DV, Lapkin AA, Plucinski PK, Friedrich JM, Walsh FC (2005) J Catal 235:10
22. Damm C, Israel G (2007) Dyes Pigments 75:612
23. Tran H, Scott J, Chiang K, Amal R (2006) J Photochem Photobio A 183:41
24. Zhang LZ, Yu JC (2005) Catal Commun 6:684
25. Vamathevan V, Amal R, Beydoun D, Low G, Mcevoy S (2002) J Photochem Photobio A 148:233
26. Liu SX, Qu ZP, Han XW, Sun CL (2004) Catal Today 93–95:877
27. Arabatzis IM, Stergiopoulos T, Bernard MC, Labou D, Neophytides SG, Falaras P (2003) Appl Catal B Environ 42:187
28. Coleman HM, Marquis CP, Scott JA, Chin S-S, Amal R (2005) Chem Eng J 113:55
29. Erzśebet Szabó-Bárdos, Erika Pétervári, Viktória El-Zein, Horváth A (2006) J Photochem Photobio A 184:221
30. Lee MS, Hong S-S, Mohseni M (2005) J Mol Catal A: Chem 242:135
31. Lassaletta G, Gonzalez-elipe AR, Justo A, Fernandez A, Ager FJ, Respaldiza MA, Soares JC, Dasilva MF, (1996) J Mater Sci 31:2325
32. Kuo Y-L, Chen H-W, Ku Y (2007) Thin Solid Films 515:3461
33. Jin M, Zhang X, Nishimoto S, Liu Z, Tryk DA, Emeline AV, Murakami T, Fujishima A (2007) J Phys Chem C 111:658
34. Herrmann J-M, Tahiria H, Ait-Ichou Y, Lassaletta G, Gonzilez-Elipe AR, Fernbdez A (1997) Appl Catal B Environ 13:219
35. Tseng I-H, Chang W-C, Wu JCS (2002) Appl Catal B Environ 37:37
36. Hou L-R, Yuan C-Z, Peng Y (2007) J Hazard Mater 139:310